

## **Modelling Material Properties Leading to the Prediction of Distortion during Heat Treatment of Steels**

Z. Guo<sup>1</sup>, N. Saunders<sup>2</sup>, A.P. Miodownik<sup>1</sup> and J.-Ph.Schillé<sup>1</sup>

<sup>1</sup> Sente Software Ltd., Surrey Technology Centre, Guildford GU2 7YG, U.K.

<sup>2</sup> Thermotech Ltd., Surrey Technology Centre, Guildford GU2 7YG, U.K.

Keywords: Material properties, heat treatment, distortion, TTT/CCT diagrams, modelling

### **Abstract**

Distortion induced by heat treatment is a major industrial problem because it critically affects the dimensional accuracy of precision components. Prediction of distortion is difficult because it requires detailed knowledge of the material properties which are normally lacking and difficult to evaluate, especially at high temperatures. The present work describes the development of a computer model for prediction of the material properties required for distortion prediction in steels. The success of the model is based on accurate description of all the major phase transformations taking place, as well as an accurate calculation of the properties of different phases formed during heat treatment. The model calculates a wide range of physical, thermophysical and mechanical properties, all as a function of time/temperature/cooling rate. Jominy hardenability prediction was also performed and shows excellent agreement with experimental data. All the present calculations can be carried out via a user friendly graphical interface.

### **Introduction**

Heat treatments are widely used in various manufacturing processes to enhance the quality of a product. However, heat treatment can generate unwanted distortion. This is a major industrial problem because it critically affects the dimensional accuracy of precision components, which may considerably increase the cost and time required for product development and decrease the quality of core parts. If distortion can be predicted and controlled, then corrections can be made during the earlier machining stage so that the components reach their final desired shape and dimension after heat treatment.

Prediction of distortion induced by heat treatment has generally been based on prior experience or by a trial and error approach. In recent years with the significant improvement of computing power, finite-element (FE) tools have been developed to tackle this problem. While being successful in some cases, almost all of the FE-modelling packages suffer from one common problem: the lack of accurate material property data. This is because distortion prediction requires detailed knowledge of the material properties as a function of alloy composition and heat treatment procedures, whereas such properties are normally unavailable especially at elevated temperatures. This problem is fatal for FE-modelling because simulation based on inaccurate material information is simply not trustworthy.

In summary, the following information on materials properties has to be known for distortion prediction:

- Phase transformation kinetics, i.e. TTT and CCT diagrams.
- Temperature and microstructure dependent thermophysical properties, such as density, thermal expansion coefficient, and thermal conductivity.
- Temperature and microstructure dependent mechanical properties, including tensile strength, yield strength, hardness, and stress-strain curves.

In the present paper, the development of a computer program is reported, which can calculate the above material properties for general steels. The success of the model is based on an accurate description of all the major phase transformations taking place during heat treatment, as well as an accurate calculation of the properties of different phases formed in steels. Jominy hardenability calculations have also been carried out to meet industrial interests. The program has been incorporated into JMatPro, a computer software for materials property simulation, which allows the required calculations to be readily carried out via a user friendly interface.

### **Phase Transformation Diagrams**

Knowledge of the TTT and CCT diagrams of steels is important for prediction of distortion since the volume change from phase transformations during heat treatment is the main factor responsible for the distortion. Much experimental work has been undertaken to determine such diagrams. However, the combination of wide alloy specification ranges, coupled with sharp sensitivity to composition changes plus a dependency on grain size, means that it is impossible to experimentally produce enough diagrams for general use.

Significant work has been undertaken over recent decades to develop models that can calculate TTT and CCT diagrams for steels.<sup>1,2,3,4,5)</sup> The pioneering work of Kirkaldy and co-workers showed that it is possible to calculate quite accurate TTT and CCT diagrams for low alloy steels.<sup>1,2)</sup> Later work by Bhadeshia used a different method to determine start curves for ferrite and bainite transformations.<sup>3,4)</sup> The model of Bhadeshia has been extended by Lee to cover slightly higher concentrations.<sup>5)</sup> However, although successful for low alloy steels these models are limited when it comes to more highly alloyed types. One of the drawbacks of both models has been the use of dilute solution thermodynamics in calculating transformation temperatures. This can now be overcome using thermodynamic models that provide high quality results for steels in general, ranging from stainless steels to tool steels as well as the low to medium alloy range types.<sup>6)</sup> The aim of the present work is to combine the more extensive thermodynamic models with a kinetic model to see if the composition range of applicability could be extended to cover a wider range of steels, including the highly alloyed types.

This goal has been achieved and JMatPro is now able to calculate TTT and CCT diagrams for steels of all types.<sup>7)</sup> The model of Kirkaldy was chosen as the basis for the new calculations as there is a clearly identifiable set of input parameters that are required and which can be readily calculated. An increased accuracy of the thermodynamic input parameters have allowed the development of an improved set of the empirical constants used in the treatment. Figure 1 shows the TTT diagrams calculated for four very different types of steels (a) a low alloy 4140 steel, (b) a high carbon, medium alloyed NiCrMo steel, (c) a T1 high speed tool steel and (d) a 13% Cr steel including comparison with experiment for all cases. While Figure 1 provides detailed results for specific alloys, it is instructive to look at the overall accuracy of the calculations. Figure 2 shows a comparison between experimentally observed times at the nose temperature of the C-curves denoting the start of transformation to ferrite, pearlite and bainite and those calculated from the model. In some cases, particularly for the fast transformation steels, it was not possible to clearly differentiate the nose temperatures for the various transformations. For example,

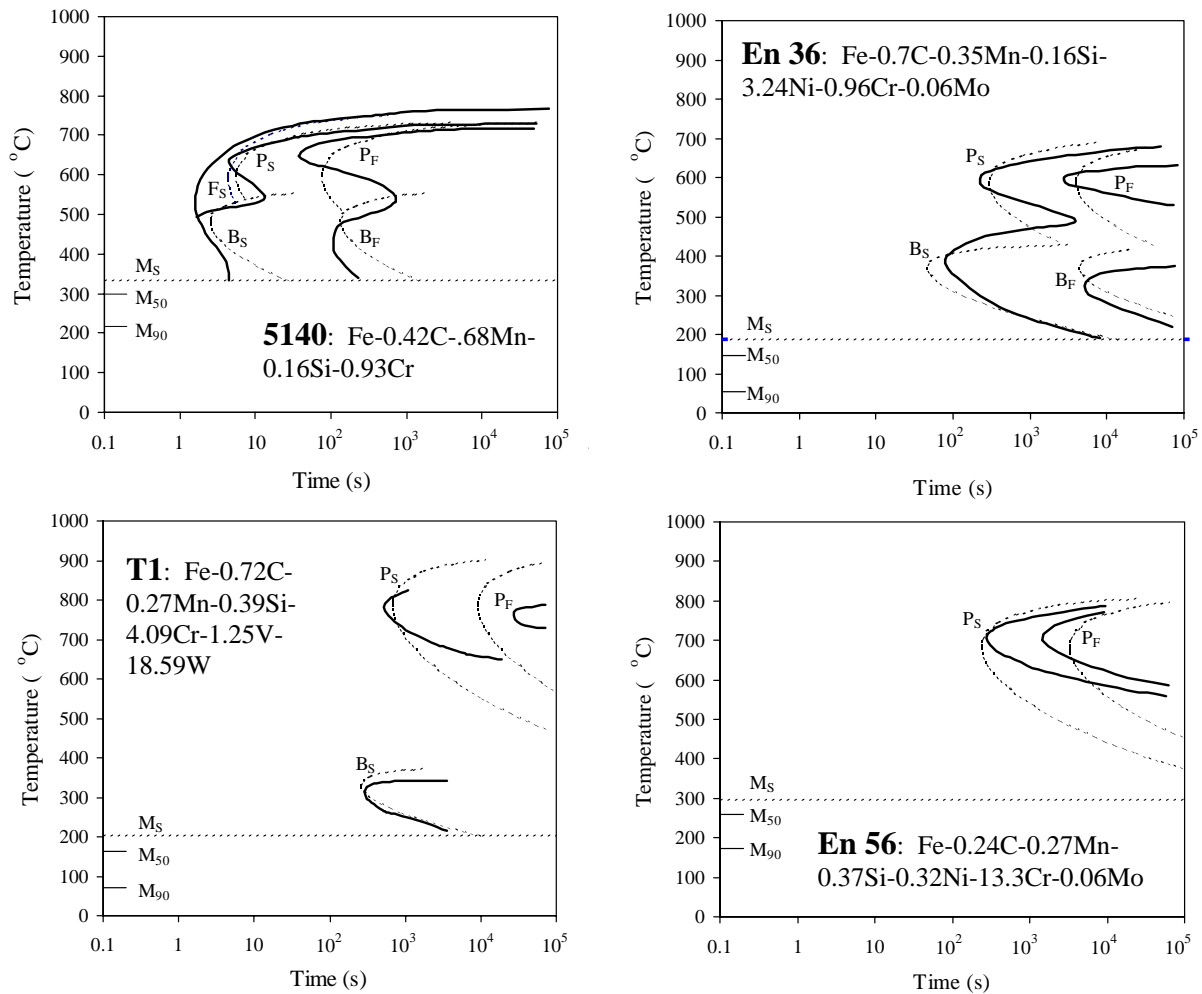


Figure 1. Comparison between experimental (solid lines) and calculated (dotted lines) TTT diagrams for various steels

the ferrite, bainite and pearlite transformations appear merged into a continuous C-curve in the experimental work. In such circumstances, the calculated transformation of the fastest phase was taken. The results have been broken down for comparison between British En steels and ASM atlas steels. The dashed lines in Figure 2 represent a deviation of 3 times. The comparison between calculation and experiment is very good and represents a substantial advance over previous models whose range of validity is largely confined to carbon and low alloy steels. Further analysis shows that 80% of calculated results are within a factor of 3 of experiment while almost 90% lie within a factor of 4. To emphasise the high levels of alloying used in the above comparison studies, Table 1 shows the maximum levels of particular elements added as well as the lowest level of Fe in any one alloy.

Table 1. Maximum level of alloying addition in steels used for validation of the model. Also shown is the minimum level of Fe.

	max/min level		max level		max level
Fe	> 75	Ni	< 8.9	W	< 18.6
C	< 2.3	Cr	< 13.3	Al	< 1.3
Si	< 3.8	Mo	< 4.7	Cu	< 1.5
Mn	< 1.9	V	< 2.1	Co	< 5.0

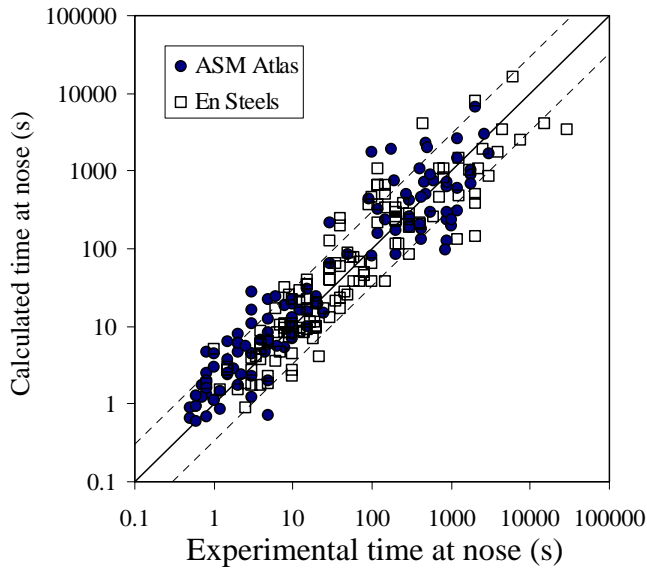


Figure 2. Comparison of calculated and experimental values for the time at nose of various C-Curves

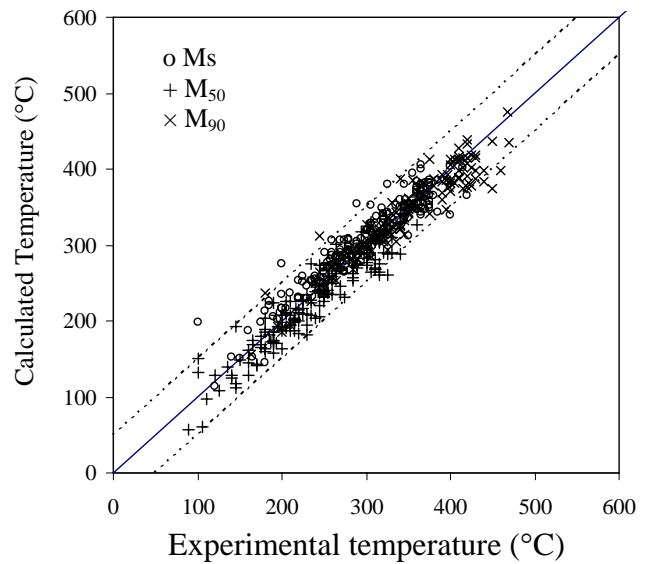


Figure 3. Comparison between experimental and calculated martensite temperatures for various steels.

An accurate description of the martensitic transformation is of great importance because of the large volume change caused by this transformation. The most commonly used formula for calculating the martensite start temperature ( $M_s$ ) is drawn from Andrews<sup>8)</sup>, which provides a good benchmark for low to medium alloy steels. Unfortunately, the accuracy of Andrew's formula falls away drastically at higher alloy contents. Recent work by Ghosh and Olson<sup>9)</sup> has attempted to extend the compositional limits to high alloy steels by using an approach linked to the  $T_0$  temperature between undercooled austenite and ferrite. While a  $T_0$  approach is theoretically favoured, it is likely that many of the problems encountered by Ghosh and Olson can be attributed to the need to incorporate a more sophisticated magnetic model for iron, which explicitly recognises the 2 gamma state electronic contribution. There are current moves to recognise this need,<sup>10)</sup> but the complex magnetic behaviour that arises through alloying<sup>11)</sup> makes its inclusion in a multi-component thermodynamic database unlikely in the near future. Therefore an essentially empirical approach to incorporating some features of the two gamma state model has been used. In addition, unlike most previous attempts the present approach incorporates certain important features of a full thermodynamic treatment, notably that each element makes a contribution to the stability of both the parent and the product phases and therefore is not treated rigidly as an austenite or ferrite (martensite) stabiliser. By combining suitable mathematical functions, the model automatically generates different behaviour of elements in different concentration ranges and in different solute environments.

The determination of the correct austenite composition is an important feature of the current integrated treatment. When carbides or other second phases are present, or when the alloy is quenched from the austenite/ferrite two-phase region, it is inappropriate to use the overall alloy composition. In the present treatment, the composition of austenite at the quench temperature is always calculated directly and used in the required model equations. It should be noted that when carbides exist at the quenching temperature, the composition used for  $M_s$  calculation should be that of the austenite phase instead of the alloy composition. Such consideration may make a big difference bearing in mind the powerful effect of interstitial carbon in suppressing  $M_s$  temperature.

The shear transformation of austenite to martensite is largely independent of time and depends only on the degree of undercooling below  $M_s$  temperature. The following equation gives a good description of the athermal transformation kinetics of martensite; it is based on the equation by Koistinen and Marburger<sup>12)</sup> with his constant made dependent on the value of  $M_s$ :

$$f_M = 1 - \exp(-c \cdot \sqrt{M_s} \cdot \Delta T) \quad (1)$$

where  $f_M$  is the volume fraction of martensite and  $\Delta T$  is the extent undercooling below  $M_s$  temperature. This enables the temperatures corresponding to 50% ( $M_{50}$ ) and 90% ( $M_{90}$ ) of martensite transformation to be determined. Figure 3 shows the comparison between experimental values<sup>13)</sup> and calculated  $M_s$ ,  $M_{50}$ , and  $M_{90}$  temperatures. As can be seen, predictions are in very good agreement with experiments.

It should be noted that the amount of martensite and bainite are each affected by changes in composition of the parent austenite, which may have resulted from any prior ferrite formation or carbide precipitation at higher temperatures. This has been considered in the present calculation of phase evolution. If there are carbides formed at the start of the transformation, then the composition used is that of the austenite in equilibrium with that carbide, instead of the alloy composition. When ferrite forms, the carbon forced out of ferrite is assumed to be evenly distributed in the remaining austenite phase. Examples given below demonstrate how cooling rate affects the physical and thermophysical properties of a steel 4140 (composition: Fe-0.98Cr-0.77Mn-0.21Mo-0.04Ni-0.15Si-0.37C, grain size ASTM 7~8). Figure 4 shows the evolution of various phases during cooling at 20 °C/s and 1 °C/s, respectively. The influence of cooling rate on phase transformations is clearly demonstrated.

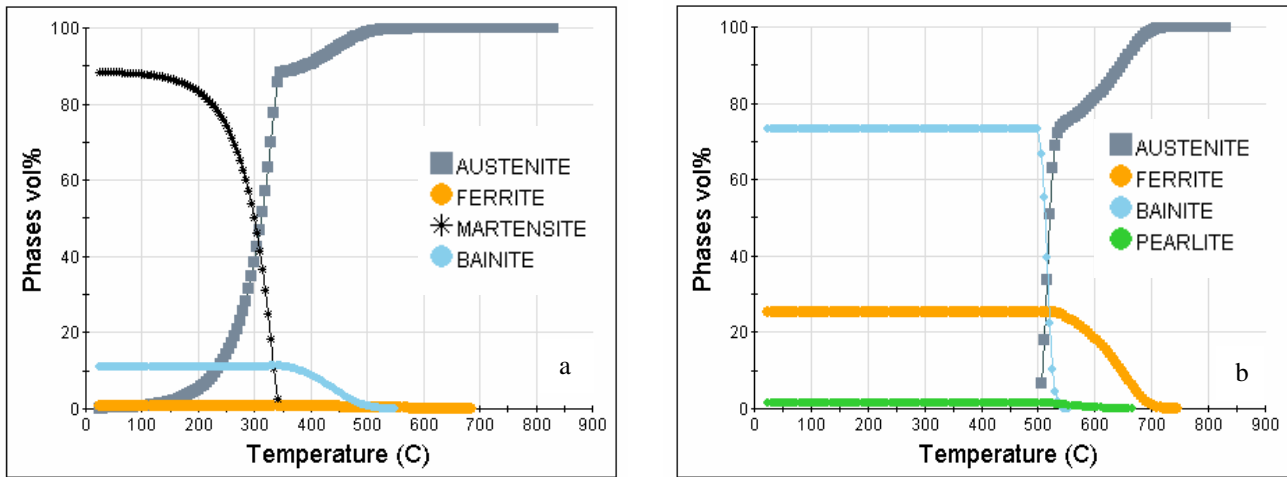


Figure 4. Microstructure evolution in 4140 during cooling at (a) 20°C/s and (b) 1°C/s

### Thermophysical and Physical Properties

Thermophysical and physical properties are critical parameters for the prediction of distortion induced by heat treatments or processing. An extensive database has been created within the development of JMatPro for the calculation of physical and thermophysical properties of various phases. For each individual phase in a multicomponent system, its properties such as molar volume, thermal conductivity, and Young's modulus are calculated using simple pair-wise mixture models, similar to those used to model thermodynamic excess functions in multi-component alloys.<sup>6)</sup>

$$P = \sum_i x_i P_i^0 + \sum_i \sum_{j>i} x_i x_j \sum_v \Omega_{ij}^v (x_i - x_j)^v \quad (2)$$

where,  $P$  is the property of the phase,  $P_i^0$  is the property of the phase in the pure element,  $\Omega_{ij}^v$  is a binary interaction parameter dependent on the value of  $v$ ,  $x_i$  and  $x_j$  are the mole fractions of elements  $i$  and  $j$  in the phase. Both  $P_i^0$  and  $\Omega_{ij}^v$  are temperature dependent. It is possible to include ternary or higher order effects where appropriate.

Once the property of each individual phase is defined, it is linked to the phase transformation calculations described in the previous section. The property of the final alloy can then be calculated using mixture models that can account for the effect of microstructure on the final property.<sup>14,15</sup> Such models, which were developed for two-phase systems, have been extended to allow calculations to be made for multiphase structures.<sup>16</sup> When the properties of the phases are similar, most types of mixture models tend toward the linear rule of mixtures. However, the power of the present models becomes apparent when phases with very different properties exist in an alloy, for instance, in the case of modulus calculations when high levels of carbides or borides are present in relatively soft metallic matrices. Extensive databases of relevant parameters exist for most of the major phases in Al, Fe, Mg, Ni, and Ti alloys. Such databases have been extensively validated against experimental measurements. Utilizing well-established relationships between certain properties (e.g., thermal and electrical conductivity) allows other properties to be calculated without using further databases, so that the

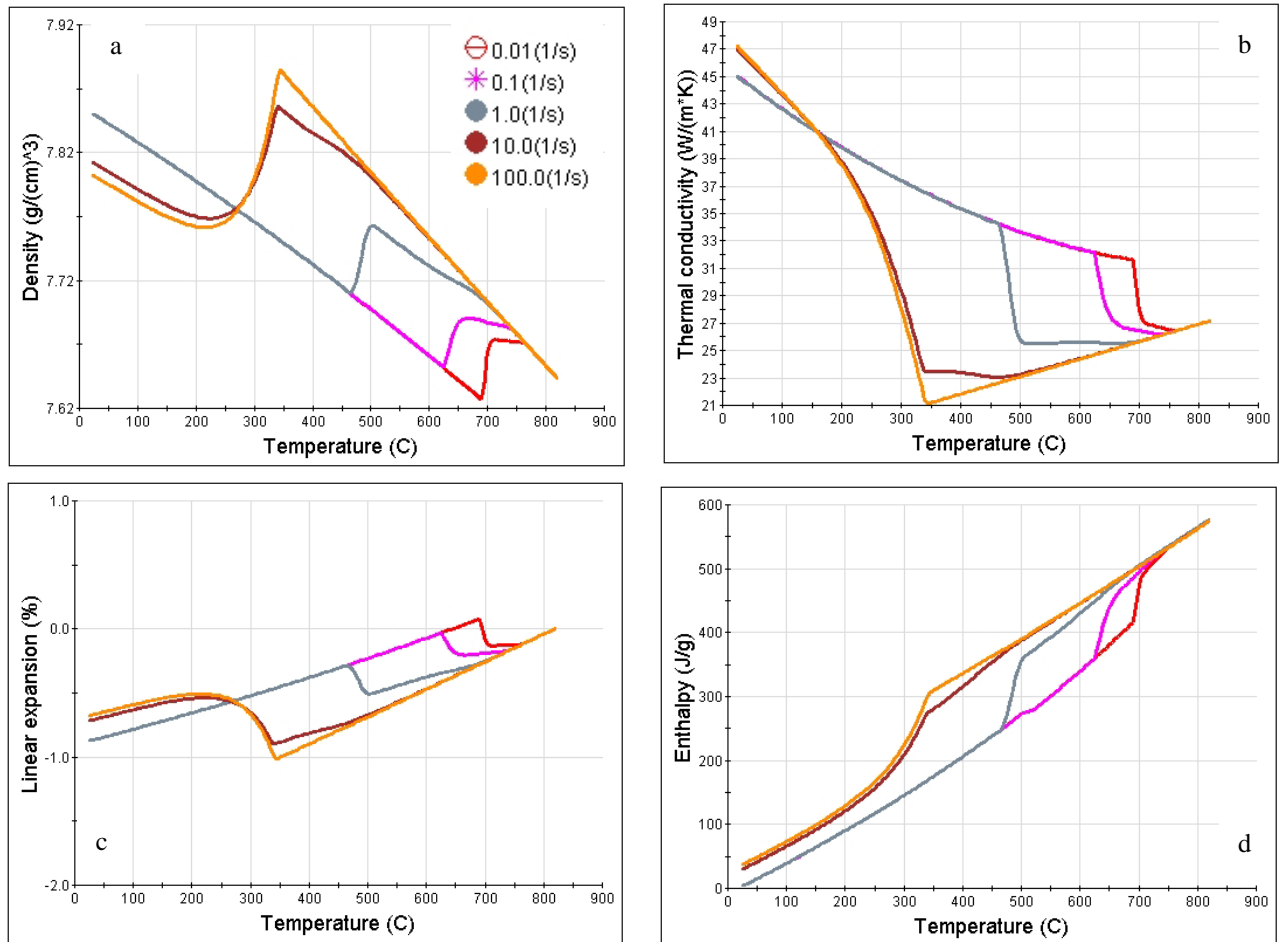


Figure 5. Various properties calculated for a 4140 steel at various cooling rates ranging from 0.01 to 100 °C/s.

following properties can be modelled: volume, density, thermal expansion coefficient, Young's, bulk and shear moduli, Poisson's ratio, thermal conductivity and diffusivity, electrical conductivity, viscosity, and resistivity.

The ability of JMatPro to model physical and thermophysical properties has been demonstrated in previous published work for various metallic systems.<sup>17)</sup> Therefore, it is not the intention of this paper to give a full detailed account of how this has been achieved. Interested readers can refer to relevant papers. One should be aware, however, that the properties reported in previous work are either for an alloy after heat treatment (assuming a frozen microstructure below the heat treatment temperature) or during the solidification process, whereas what is going to be demonstrated in this paper is the change of these properties during heat treatment, i.e. to monitor the temperature and microstructure sensitivity of these properties. Once the kinetics of major phase transformations in steels are known, the calculation of material properties during heat treatment is straightforward. First, one calculates the phase evolution during the heat treatment of concern: isothermal holding, continuous cooling, or any complex cooling path resulting from modern heat treatments. Then by combining the phase constitution with JMatPro's capabilities for calculating the properties of each phase, the overall properties of the alloy during heat treatment can be obtained. Examples given below demonstrate how cooling rate affects the physical and thermophysical properties of the steel 4140 used in the previous section. Five cooling rates are set as 100, 10, 1, 0.1, 0.01 °C/s respectively.

Typical physical and thermophysical properties relevant to the prediction of distortion such as density, linear expansion coefficient, thermal conductivity and enthalpy at different cooling rates are plotted in Figure 5. The properties at 100°C/s and 10°C/s are very close, because the proportion of martensite is over 90% in both cases. Figure 6 shows the comparison between the calculated and experimental quench strain for a 5140 steel, and the error is less than 10%.

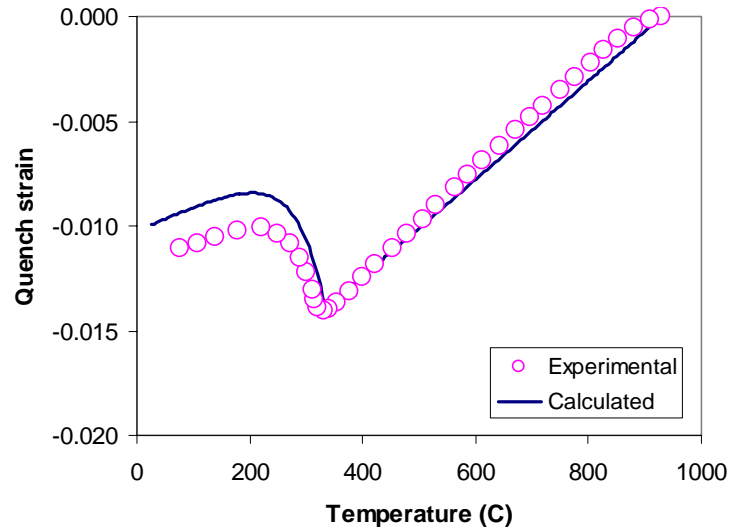


Figure 6. Comparison between the calculated and experimental quench strain for a 5140 steel

### Mechanical Properties During Heat Treatment

The mechanical properties of steels during heat treatment can be calculated following similar procedures to those described in the previous section. Before doing so, the hardness of various phases such as martensite and bainite has to be calculated. Expressions were developed to relate hardness to composition and cooling rate based on the experimental data covering a wide composition range. Figure 7 demonstrates the accuracy of the calculations in comparison with experimental values, using martensite as an example. For austenite and ferrite phases, the strengthening model in JMatPro utilises a generalised pair interaction approach for solid solution strengthening.<sup>18)</sup> The classic Hall-Petch equation is employed to account for the dependence of strength on grain size. Using steel 4140 as an example, the influence of cooling rate on yield strength and hardness is shown in Figure 8. The strength

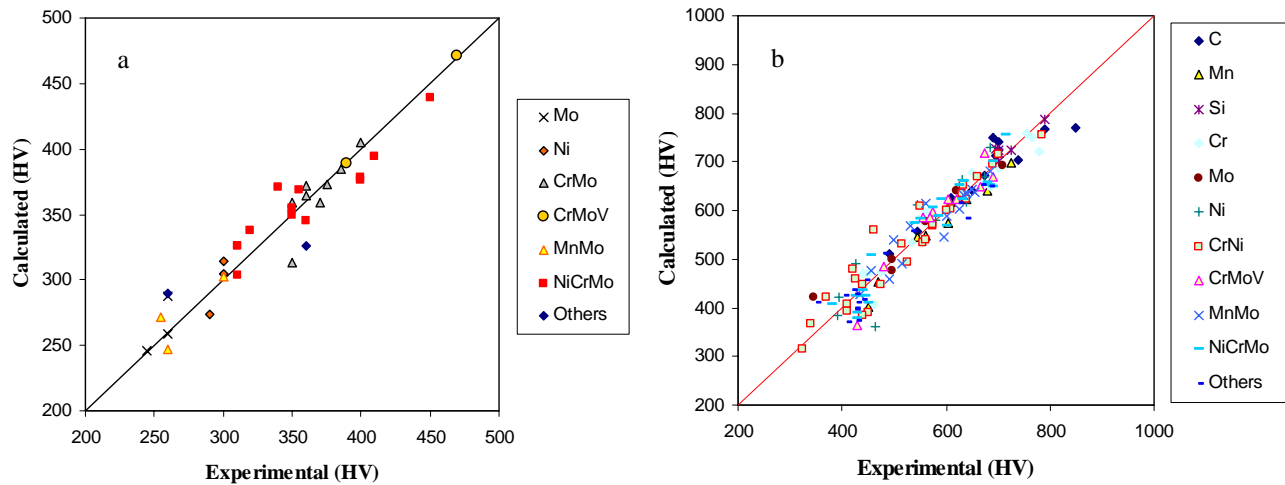


Figure 7. Comparison between experimental and calculated hardness for (a) bainite, and (b) martensite

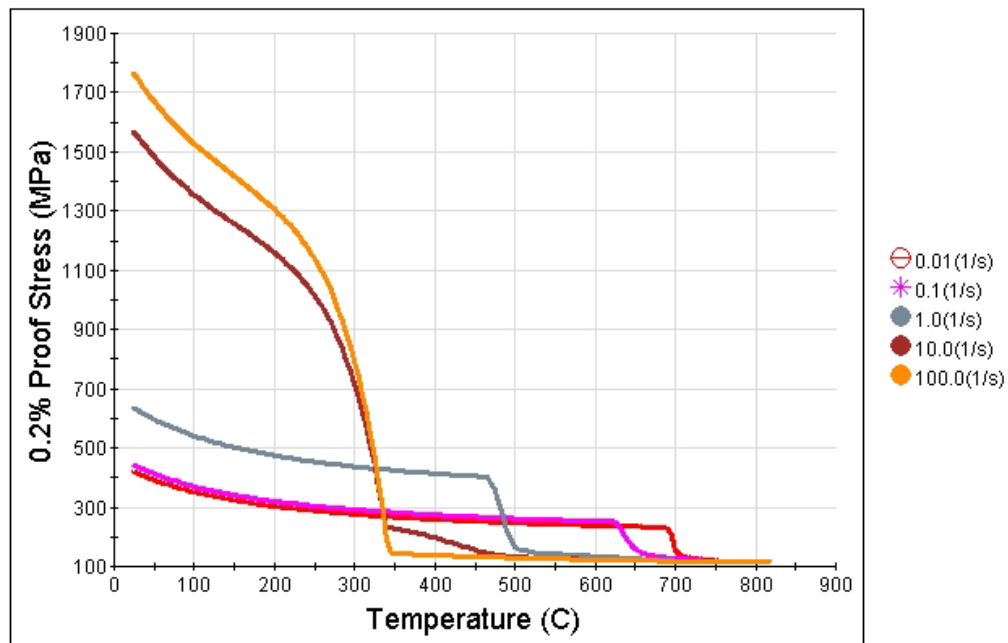


Figure 8. Yield stress for a 4140 steel at various cooling rates ranging from 0.01 to 100 °C/s.

properties at 100 and 10 °C/s are very close due to the fact that the majority phase is martensite in both cases.

Compared with cooling at a constant rate, Jominy end-quench test results are associated with a more complicated cooling pattern. Accurate prediction of Jominy hardenability curve is therefore of great challenge and importance. The major steps of predicting Jominy hardness using this model are as follows:

- computing equilibrium phase transformation temperatures and phase composition using a thermodynamic model for the multi-component equilibria in heat treatable steels;
- calculating the cooling profile for a certain position along the Jominy quenching bar;

- computing the microstructure evolution at each position along the Jominy bar using transformation kinetics models for austenite decomposition, i.e. the formation of ferrite, pearlite, bainite and martensite; and
- calculating hardness for a certain position along the Jominy quenching bar.

Again using steel 4140 as an example, the Jominy hardenability curve was calculated and compared with the experimental curve in Figure 9(a)<sup>19)</sup> As can be seen that the two curves agree very well.

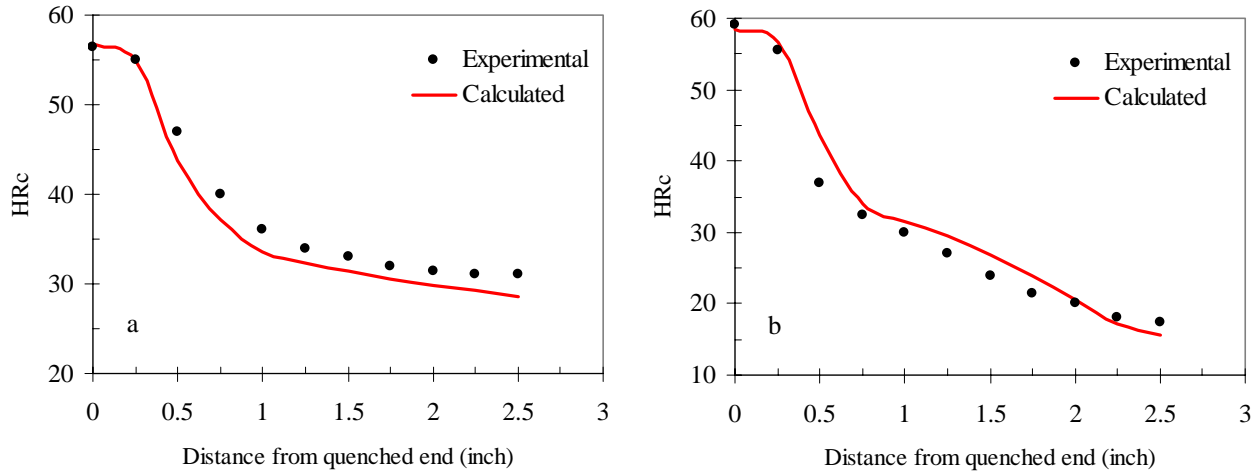


Figure 9. Jominy hardenability comparison between experimental and calculated curve for a) 4140, and b) 5140 alloys

The Jominy hardenability curve of another alloy 5140 (Fe-0.42C-0.93Cr-0.68Mn-0.16Si, ASTM grain size 6.5) was also calculated and agrees well with experimental measurement, Figure 9(b). The curve exhibits two zones: a fast hardness drop from quenching end to 0.75 inch depth, and a slow hardness drop between 0.75 and 2.5 inches. This behaviour can be readily explained by the microstructure change along the Jominy quench bar, Figure 10. It can be seen that the initial fast hardness drop is mainly due to the formation of bainite at the expense of martensite. At depth over 0.75 inch, pearlite starts to form at the expense of bainite (the stronger of the two phases), which leads to the second slow drop in hardness.

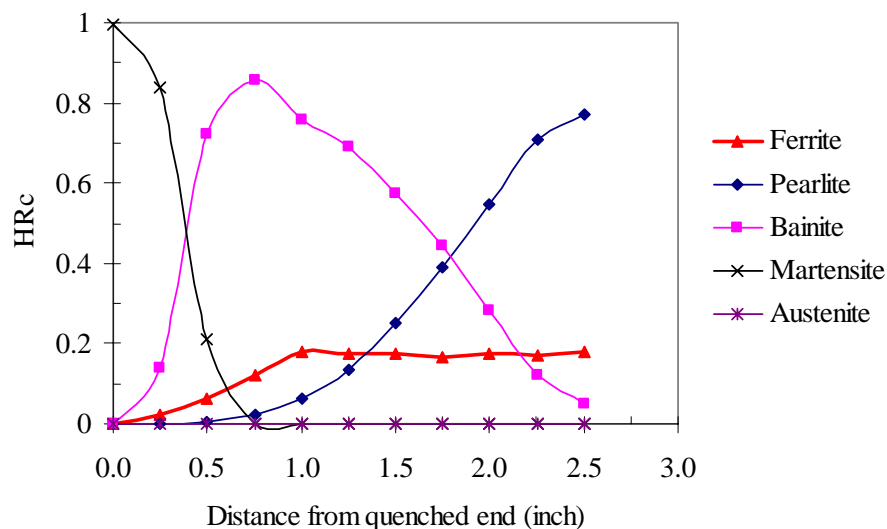


Figure 10. Microstructure change along the Jominy quench bar for a 5140 alloy

## Summary

Properties critical to the prediction of distortion induced by heat treatment have been calculated using JMatPro, which embodies new software for materials property simulation and displays the results via a user friendly interface. These properties include TTT and CCT diagrams, physical, thermophysical and mechanical properties, including those at high temperatures, which are normally unavailable. The success of the model is based on accurate description of all the major phase transformations taking place, as well as an accurate calculation of the properties of different phases formed during heat treatment process. The model calculates a wide range of physical, thermophysical and mechanical properties, all as a function of time/temperature/cooling rate or any arbitrary cooling profile. Jominy hardenability prediction for some specific steels have been used as examples.

## REFERENCES

- 1) J.S. Kirkaldy, B.A. Thomson, and E.A. Baganis, Hardenability Concepts with Applications to Steel, eds. J.S. Kirkaldy and D.V. Doane, (Warrendale, PA: AIME, 1978), 82
- 2) J.S. Kirkaldy and D.Venugopalan, Phase Transformations in Ferrous Alloys, eds. A.R. Marder and J.I. Goldstein, AIME, (Warrendale, PA: AIME, 1984), 125
- 3) H.K.D.H. Bhadeshia, *Met. Sci.* **15** (1981) 175
- 4) H.K.D.H. Bhadeshia, *Met. Sci.* **16** (1982) 159
- 5) J.L. Lee and H.K.D.H. Bhadeshia, *Mater. Sci. Eng. A* **171** (1993) 223
- 6) N. Saunders and A.P. Miodownik, CALPHAD – Calculation of Phase Diagrams, Pergamon Materials Series vol.1, (Ed.: R.W. Cahn), Elsevier Science, Oxford, 1998
- 7) N. Saunders et al., Sente Software Ltd., Guildford GU2 7YG, U.K. 2004
- 8) K.W. Andrews, *J. Iron & Steel. Inst.*, **183** (1965) 721
- 9) G. Ghosh and G.B. Olson, *J. Phase Equilibria*, **22** (2001) 199
- 10) Q. Chen and B. Sundman, *J. Phase Equilibria*, **22** (2001) 631
- 11) D. de Fontaine et al., *CALPHAD*, **19** (1995) 499
- 12) D.P. Koistinen and R.E. Marburger, *Acta Metall.* **7** (1959) 59
- 13) M. Atkins, Atlas of Continuous Cooling Transformation Diagrams for Engineering Steels, Sheffield, British Steel Corporation, 1977
- 14) Z. Fan, P. Tsakiroopoulos and A.P. Miodownik, *J. Mat. Sci.*, **29** (1994) 141
- 15) Z. Fan, *Phil. Mag. A*, **73** (1996) 1663
- 16) A.P. Miodownik et al., unpublished research, Sente Software Ltd., Guildford GU2 7YG, U.K.
- 17) <http://www.sentesoftware.co.uk/biblio.html> (papers on JMatPro downloadable in pdf format)
- 18) X. Li, A.P. Miodownik and N. Saunders, *Mater. Sci. Technol.* **18** (2002) 861
- 19) American Society for Metals, Atlas of Isothermal Transformation and Cooling Transformation Diagrams, Metals Park, Ohio, 1977